# Change of Multifractal Thermal Characteristics in the Western Philippine Sea Upper Layer During Internal Wave-Soliton Propagation

Peter C Chu, Chung-Ping Hsieh
Naval Ocean Analysis and Prediction Laboratory, Naval Postgraduate School
Monterey, California 93940

# Report Documentation Page

*Form Approved*
*OMB No. 0704-0188*



| 1. REPORT DATE | 2. REPORT TYPE | 3. DATES COVERED |
|---|---|---|
| **2007** | | **00-00-2007 to 00-00-2007** |

| 4. TITLE AND SUBTITLE | 5a. CONTRACT NUMBER |
|---|---|
| **Change of Multifractal Thermal Characteristics in the Western Philippine Sea Upper Layer During Internal Wave-Soliton Propagation** | 5b. GRANT NUMBER |
| | 5c. PROGRAM ELEMENT NUMBER |
| 6. AUTHOR(S) | 5d. PROJECT NUMBER |
| | 5e. TASK NUMBER |
| | 5f. WORK UNIT NUMBER |
| 7. PERFORMING ORGANIZATION NAME(S) AND ADDRESS(ES) **Naval Postgraduate School,Department of Oceanography,Monterey,CA,93943** | 8. PERFORMING ORGANIZATION REPORT NUMBER |
| 9. SPONSORING/MONITORING AGENCY NAME(S) AND ADDRESS(ES) | 10. SPONSOR/MONITOR'S ACRONYM(S) |
| | 11. SPONSOR/MONITOR'S REPORT NUMBER(S) |

12. DISTRIBUTION/AVAILABILITY STATEMENT
**Approved for public release; distribution unlimited**

13. SUPPLEMENTARY NOTES

14. ABSTRACT

15. SUBJECT TERMS

| 16. SECURITY CLASSIFICATION OF: | | | 17. LIMITATION OF ABSTRACT | 18. NUMBER OF PAGES | 19a. NAME OF RESPONSIBLE PERSON |
|---|---|---|---|---|---|
| a. REPORT **unclassified** | b. ABSTRACT **unclassified** | c. THIS PAGE **unclassified** | **Same as Report (SAR)** | **35** | |

## Abstract

Upper layer (above 140 m depth) temperature in the western Philippine Sea near Taiwan was sampled using a coastal monitoring buoy (CMB) with attached 15 thermistors during July 28 – August 7, 2005. The data were collected every 10 min at 1, 3, 5, 10, 15, and 20 m using the CMB sensors, and every 15 sec at 15 different depths between 25 m and 140 m. Internal waves and solitons were identified from the time-depth plot of the temperature field. Without the internal waves and solitons, the power spectra, structure functions, and singular measures (representing the intermittency) of temperature field satisfy the power law with multi-scale characteristics at all depths. The internal waves do not change the basic characteristics of the multifractal structure. However, the internal solitons change the power exponent of the power spectra drastically especially in the low wave number domain; break down the power law of the structure function; and increase the intermittency parameter. The physical mechanisms causing these different effects need to be further explored.

# 1. Introduction

Theories of turbulence as applied to point measurements in ocean drifting buoy concern the scaling properties, in a statistical sense, of differenced time series, where the Taylor hypothesis is invoked so that the difference between measurements at some time $t$ and a later time $t+\tau$ acts as a proxy for the difference between measurements made at two points in the fluid separated by length scale $l$. For a time series $T(x_i)$ with an evenly spaced interval $l$ and a total length $L$,

$$T_i = T(x_i), \quad x_i = il, \quad i = 0,1,...,\Lambda, \quad L = \Lambda l ,$$

an increment series

$$|\Delta T(x_i, rl)| = |T(x_{i+r}) - T(x_i)|, \quad i = 0,1,...,\Lambda - r \tag{1}$$

can be constructed with respect to the increment $rl$ ($r$ is an integer).

Studies of scaling in upper ocean turbulence have focused on the power spectra and the structure functions (see e.g. Chu 2004). The $q$-th order structure function is defined by

$$S(r,q) \equiv \left\langle \left|\Delta T(x, rl)\right|^q \right\rangle = \frac{1}{\Lambda - r}\sum_{i=0}^{\Lambda - r}\left|\Delta T(x_i, rl)\right|^q . \tag{2}$$

Here, $r$ is inversely proportional to the wavenumber $l$,

$$r \propto \frac{1}{l}.$$

Obviously, for small $r$, $\Delta T(x_i, rl)$ represents the small-scale fluctuations (usually turbulence). The first-order structure function $S(r, 1)$ was initially introduced for studying small-scale turbulence where it appeared to be an effective tool in linking turbulence physics with statistics. The scale-invariance of the variable $T$ is represented by

$$\left|\Delta T(x_i, l)\right| = r^{-H} \left|\Delta T(x_i, rl)\right|, \tag{3}$$

where $H$ is the scaling exponent, or called the Hurst exponent. In 1941, Kolmogorov suggested that the velocity increment in high-Reynolds number turbulent flows should scale with the mean (time-averaged) energy dissipation and the separation length scale. The Hurst exponent $H$ is equal to 1/3. For the $q$-th order structural function, the simple self-similarity means

$$\left\langle \left|\Delta T(x_i, l)\right|^q \right\rangle = r^{-qH} \left\langle \left|\Delta T(x_i, rl)\right|^q \right\rangle. \tag{4}$$

Multifractal behavior may be generalized from (4) into

$$\left\langle \left|\Delta T(x_i, l)\right|^q \right\rangle = r^{-\zeta(q)} \left\langle \left|\Delta T(x_i, rl)\right|^q \right\rangle. \tag{5}$$

In other words, the simple self-similarity may be described with a single scaling exponent $H$ while the multifractal scale-invariance requires a spectrum of scaling exponents with

$$\zeta(q) \neq qH .$$

In the case of multifractality, $\left\langle \left|\Delta T(x_i, l)\right|^q \right\rangle$ does not scale in the same way as $\left\langle \left|\Delta T(x_i, l)\right| \right\rangle^q$, which would be the case for simple self-similarity. With the above consideration, the scaling behavior of the structure function may be expressed by

$$S(r, q) \sim r^{\zeta(q)}, \tag{6}$$

with the spectral exponent $\zeta(q)$ independent on the mechanism of energy input. The ensemble of $\Delta T(x_i, rl)$ is invariant under translations and rotations for length scale smaller than the scale of the energy input.

The multifractal scaling characteristics of the upper layer thermal structure were found for the southwestern Greenland Sea, Iceland Sea, and Norwegian Sea (GIN Sea)

using high-resolution, digital thermistor chain data from the surface to 140 m deep. Linear dependence of $Log_2$ [$S(r, q)$] on $Log_2(r)$ is found with different $q$-values from 0.5 to 4.0 (Chu, 2004).

Does the multifractal scaling occur in other seas such as the western Philippine Sea (WPS) near Taiwan (Fig. 1)? This is the region that the Philippines Current flows northward from just north of Mindanao (the southernmost of the main island groups of the Philippines) at around (10°N, 128°E) to Taiwan where it continues as the Kuroshio - the most evident western boundary current in the North Pacific Ocean. After becoming the Kuroshio, it makes a slight excursion into the South China Sea through the Luzon Strait, continues northward, and is fed from the North Equatorial Current, from which it continues to entrain water along its way. This current system has various stages of modification that transports warm water to the North Pacific. Because of the import and modification of water masses a large number of regional water types can be encountered. Eddy activity is often observed in WPS near Taiwan. For example, a large warm eddy lies east of the Luzon Strait, a seemingly permanent feature (Nitani, 1972; Chu and Li, 2000; Chu and Fan, 2001). Although the WPS is the only important source of open-ocean water to the South China Sea, the hydrographic and chemical properties of the waters on both side of the Luzon Strait are quite different (Nitani, 1972). When the Kuroshio branches out near the southern tip of Taiwan, part of the Kuroshio intrudes into the South China Sea through the Luzon Strait. The internal tides and internal waves are probably generated by the shallow ridges in the Luzon Strait (Liu et al., 1998). During the Asian Seas International Acoustics Experiment for the South China Sea, a moored array of current, temperature, conductivity, and pressure sensors was deployed across the

Chinese continental shelf and slope. The dominant oceanographic signal by far was in fact the highly nonlinear internal waves (or solitons) which were generated near the Batan Islands in the Luzon Strait and propagated 485 km across deep water to the observation region (i.e., northern South China Sea) (Ramp et al., 2004).

Since highly nonlinear internal waves (or solitons) often occur in the Kuroshio region near Taiwan, one may ask: Does the multifractal scaling exist in the upper layer thermal field? What are the effects of internal wave and soliton propagation? To get turbulence and internal wave/soliton signals, we need high temporal resolution data with relatively long duration. Recently, a coastal monitoring buoy (CMB) with attached 15 thermistors at various depths was deployed by the U.S. Naval Oceanographic Office in WPS (Fig. 2) during July 28 – August 7, 2005. The sampling rate of the thermistors is one per 15 s. These observations provide useful data for investigating the multifractal feature of the upper layer of WPS with the presence of internal waves and solitons.

## 2. Data Description

The original design of CMB is to collect the data every 10 min near the air-ocean interface (Chu and Hsieh, 2007). Above the ocean surface, the surface winds, air temperature, and air pressure are measured. Below the ocean surface, the temperature is observed at 1, 3, 5, 10, 15, and 20 m. During the observational period (July 28 – August 7, 2005) the CMB travels 229.14 km along the track (Fig.2) with an average speed of 3.82 m per 15 sec. The surface winds are weak (around 4 m/s) and the surface air temperature is close to the water temperature at 1 m depth (implying weak buoyancy flux across the air-ocean interface). Weak surface winds and buoyancy fluxes make shallow surface mixed layer.

Fifteen thermistors are attached to a wire rope extending from the code of CMB (20 m deep) to 140 m with high frequency sampling rate (every 15 sec) (Fig. 3). Time-depth cross section of temperature along the CMB track shows a multi-scale variability with highly irregular nature (Fig. 4). The surface mixed layer is very thin (depth around 5 m) on July 28 with temperature about 28.5$^{o}$C. Below the surface mixed layer, two thermoclines appear with the first thermocline to the depth of 50 m. The vertical gradient in the first thermocline is around 0.1$^{o}$C/m. A relatively uniform sublayer (24$^{o}$C) exists below the first thermocline from 50 to 130 m. Below the uniform sublayer, there is a second thermocline with a vertical temperature gradient around 0.04$^{o}$C/m. As time approaches, the surface mixed layer deepens and the first thermocline descends. These processes contain small scale fluctuations. The surface mixed layer reaches 70 m on August 5, when an evident cooling occurs with the mixed layer temperature reducing to 25.5$^{o}$C. At the same time, the two thermoclines merge to a single themocline with the vertical gradient of 0.06$^{o}$C/m.

## 3. Temperature Anomaly

During the temperature sampling from CMB thermistors (Fig. 4), temperature anomaly in the upper layer can be calculated by

$$T'(t,z) = T(t,z) - \bar{T}(z), \tag{7}$$

which is the deviation of the observed temperature from the temporally mean temperature. Without salinity data, the isopycnal displacement is calculated by (Desaubles and Gregg, 1981)

$$\eta(t,z) = -\frac{T'(t,z)}{d\bar{T}/dz}, \tag{8}$$

which fluctuates with various amplitudes ($A_\eta$). Three types can be identified due to the magnitude of $A_\eta$: (a) turbulence-dominated type ($A_\eta \leq 5$ m), (b) internal wave (IW) – turbulence type ($5\text{ m} < A_\eta \leq 30\text{ m}$), and (c) internal soliton (IS) – turbulence type ($A_\eta > 30$ m). During the whole observational period (28 July to 7 August 2005), the IS-turbulence type occurs only on 0700-1200 GMT July 30, 2005 (Fig. 4). Two 5-hr durations before and after the occurrence of the IS-turbulence type are chosen for the comparison (Fig. 5): 1000-1500 GMT July 29, 2005 (IW-turbulence type), and 0000-0500 GMT August 1 (turbulence-dominated type). During the remaining six days (0500 GMT August 1 to 7 August 2005), the IW-turbulence type occurs more often than the turbulence-dominated type.

Since the upper ocean is usually turbulent due to mixing, the turbulence-dominated, IW-turbulence, and IS-turbulence types are regarded as lack of internal waves, existence of internal waves, and existence of internal solitons. Thus generation, growth, propagation, and dissipation are the factors controlling the alternative occurrence of IW-turbulence, IS-turbulence and turbulence-dominated types. Generation of internal waves is most often attributed in some way to tidal flow across abrupt topography (Ramp et al., 2004). Lacking *in situ* information at the generation site to describe the dynamics, this manuscript will focus mainly on describing the change of the multifractal thermal structure with the propagation of internal waves and internal solitons.

For the IW-turbulence type (1000-1500 GMT July 29, 2005, Fig. 6a), the maximum temperature fluctuation decreases with depth from $\pm 1.6^o C$ at the surface to $\pm 0.4^o C$ at 100 m deep and then increases with depth to $\pm 1^o C$ at 140 m deep. For the IS-turbulence type (0700-1200 GMT July 30, 2005, Fig. 6b), the maximum temperature

fluctuation increases with depth from $\pm 1.8^{o}C$ at the surface to $\pm 2.9^{o}C$ at 60 m deep, then decreases with depth to $\pm 0.8^{o}C$ at 100 m deep, and finally increases with depth to $\pm 2.1^{o}C$ at 140 m deep. For the dominant-turbulence type (0000-0500 GMT August 1, Fig. 6c), the maximum temperature fluctuation decreases with depth from $\pm 1.3^{o}C$ at the surface to $\pm 0^{o}C$ at 60-65 m deep, and then increases with depth to $\pm 0.9^{o}C$ at 140 m deep.

The observed temperature profile oscillates during the IW-turbulence type (1000-1500 GMT July 29, Fig. 7a) and IS-turbulence type (0700-1200 GMT July 30, Fig. 7b), but not in the turbulence-dominated type (0000-0500 GMT, August 1). The oscillation is evident in the upper layer above 50 m in the IW-turbulence type and above 80 m in the IS-turbulence type. This may be related to the different descending of the first thermocline with 80 m for the IS-turbulence type and 50 m for the IW-turbulence type (Fig. 4). Besides, the amplitude of the oscillation is much larger in the IS-turbulence type (maximum amplitude around $4^{o}$C) than the IW-turbulence type (maximum amplitude around $2^{o}$C). For the IS-turbulence type (Fig. 7b), oscillation of the temperature profiles can be found from 15 thermistors with 7 min apart from 0752 to 0827 GMT July 30, 2005. Among them, the black curve is the mean temperature profile over the whole CMB track [i.e., $\overline{T}(z)$]. The temperature profile on 0752 GMT (blue curve) represents cool upper layer with the temperature of $25.3^{o}$C at 25 m depth (minimum among the five profiles). Seven min later (0757 GMT), the profile (green curve) represents warm upper with the temperature of $28.7^{o}$C at 25 m depth (maximum among the five profiles). Fourteen min later, the profile (red curve) shifts to the cool upper layer.

## 4. Isopycnal Displacement

The isopycnal displacement $\eta(t,z)$ at four different depths (40 m, 45 m, 55 m, and 60 m) is used for illustration. During the IW-turbulence type (1000-1500 GMT July 29, Fig. 8a), the isopycnal displacement oscillates with time and has maximum downwelling (20 m) at all the four depths at 1200 GMT July 29, 2005 (Fig. 8a). For the IS-turbulence type (0700-1200 GMT July 30, Fig. 8b), the amplitude of isopycnal displacement $\eta(t,z)$ is around 50 m at 45 and 50 m depths and increases to near 100 m at 60 m depth with frequency around 4 CPH. For the turbulence-dominated type (0000-0500 GMT August 1, Fig. 8c), the isopycnal displacement is very small with maximum amplitude around 4-6 m.

Similar to temperature profile, the isopycnal displacement profile oscillates in the IW-turbulence type (1000-1500 GMT July 29, Fig. 9a) and IS-turbulence type (0700-1200 GMT July 30, Fig. 9b), but not in the turbulence-dominated type (0000-0500 GMT, August 1, Fig. 9c). The oscillation is evident in the upper layer above 50 m in the IW-turbulence type and above 80 m in the IS-turbulence type. The amplitude of the oscillation is much larger in the IS-turbulence type (maximum amplitude around 100 m) than the IW-turbulence type (maximum amplitude around 20 m).

Fig. 9b shows time evolution of the isopycnal displacement profiles with 7 min apart from 0752 to 0827 GMT July 30, 2005. On 0752 GMT (blue curve), the profile represents upward displacement with maximum value of 20 m at 30 m depth. Seven min later (0757 GMT), the profile (green curve) represents downward displacement with maximum value of -100 m at 60 m depth. Fourteen min later, the profile (red curve) represent weak displacement.

## 5. Power Spectra

The energy spectra of the isopycnal displacement ($\phi_\eta$) is related to the temperature variance spectra ($\phi_T$) by

$$\phi_\eta = \left\langle \frac{d\bar{T}}{dz} \right\rangle^{-2} \phi_T . \tag{9}$$

Since the statistical features of isopycnal displacement and temperature are related to each other, we just investigate the difference of statistical structure of temperature field among IW-turbulence, IS-turbulence, and turbulence-dominated types.

Determination of the stationarity is the first step toward understand the inherent thermal variability and statistical properties identified from this high-resolution temperature data with multi-layer structures. As mentioned in Section 2, the CMB collects the data every 15 sec and travels with an average speed of 3.82 m per 15 sec. For a given depth, the temperature data is a function of the horizontal coordinates, *x*, $T_i = T(x_i), \quad x_i = il,$ and $l$ = 3.82 m. For each of the three types (IW-turbulence, IS-turbulence, and turbulence-dominated), there are 1,200 temperature profiles ($\Lambda$ = 1,200).

Spectral analyses of temperature field,

$$E_j = E(k_j), \quad k_j = j/L, \quad j = 1, 2, ..., \Lambda/2, \quad L = \Lambda l \tag{10}$$

at all depths for each type are conducted, but for the sake of brevity and to elucidate the important points, only spectra at 60 m depth are shown in Fig. 10. A Bartlett window was used to taper the ends of each series before calculating the power spectra to reduce the spectral leakage in the wavenumber domain.

For a scaling process, one expects power law behavior (Chu, 2004; Chu et al., 2002),

$$E(k) \propto k^{-\beta}, \tag{11}$$

over a large range of wavenumber $k$. The spectral exponent $\beta$ contains information about the degree of stationarity of the data. If $\beta < 1$, the field is stationary; if $1 < \beta < 3$, the field contains nonstationary signal with stationary increments and in particular, the small-scale gradient field is stationary; if $\beta > 3$, the field is nonstationary with nonstationary increments.

The power spectra for the IW-turbulence (Fig. 10a) and turbulence-dominated type (Fig. 10c) have similar multi-scaling characteristics with almost the same spectral exponent $\beta$: around 0.4 (stationary) for low wavenumbers ($\log_2 kL/2 < 4$), and nearly 5/3 (non-stationary with stationary increment) for high wavenumbers ($\log_2 kL/2 > 4$). However, the power $E(k)$ is much larger for the IW-turbulence type than the turbulence-dominated type. This implies that the energy is distributed in all wavenumbers during the internal wave propagation.

The spectrum for the IS-turbulence type (Fig. 10b) is quite different from the two other spectra especially in the spectral exponent $\beta$: around 0.4 (stationary) for low wavenumbers ($\log_2 kL/2 < 3.5$), nearly 4.2 (non-stationary with non-stationary increment) for mid-range wavenumbers ($3.5 < \log_2 kL/2 < 6$), approximately 5/3 (non-stationary with -stationary increment) for high wavenumbers ($\log_2 kL/2 > 6$).

## 6. Structure Functions

The structure function (2) is computed for the three types: (a) IW-turbulence (1000-1500 GMT July 29), (b) IS-turbulence (0700-1200 GMT Jul 30), and (c) turbulence-dominated (0000-0500 GMT August 1) types. Near-linear dependence of $\mathrm{Log}_2\,[S(r, q)]$ on $\mathrm{Log}_2(r)$ is found with different $q$-values from 1 to 6 for the IW-

turbulence type (Fig. 11a) and turbulent-dominated type (Fig. 11c), i.e., the structure function $S(r, q)$ satisfies the power law (6) with the exponent $\zeta(q)$ only depending on $q$. The power of the structure function $\zeta(q)$ is monotonically and near-linearly increasing with $q$. However, the structure function $S(r, q)$ for the IS-turbulence type does not satisfy (6) (Fig. 11b). The power law is broken approximately at $r$ = 8 min, which is nearly half period of the IS (with frequency of 4 CPH). This phenomenon occurs at all depths.

Fig. 12 shows the dependence of the structure function's power, $\zeta(q)$, on $q$ and depth for (a) 1000-1500 GMT July 29 (IW-turbulence), and (b) 0000- 0500 GMT August 1 (turbulence-dominated), 2005. For $q \le 1$, there is not much difference between the two types. The difference becomes evident as $q$ increase. For $q$ = 6, the power $\zeta(q)$ varies from 0.5 to 2.1 for the turbulence-dominated type, but from 1.2 to 3.0 for the IW-turbulence type. This indicates that the internal waves increase the power of the structure function especially for high moments. This may be related to the higher energy in each mode for the IW-turbulence type than the turbulence-dominated type (Figs. 10a, c).

## 7. Singular Measures

Normalized small scale absolute gradient

$$\varepsilon(x_i, l) = \frac{\left|\Delta T(x_i, l)\right|}{\left\langle\left|\Delta T(x_i, l)\right|\right\rangle}, \qquad \left\langle\left|\Delta T(x_i, l)\right|\right\rangle = \frac{1}{\Lambda}\sum_{i=0}^{\Lambda-1}\left|\Delta T(x_i, l)\right|, \tag{13}$$

is used to identify the intermittency (or subject to periodic stopping) of the thermal field. The running average of $r$ normalized values are computed by

$$\varepsilon(x_i, rl) = \frac{1}{r}\sum_{j=i}^{i+r-1}\varepsilon(x_j, l), \qquad i = 0,1,..., \Lambda - r\,. \tag{14}$$

The mean of the $q$th power of $\varepsilon(x_i, rl)$

$$M(r,q) \equiv \left\langle \varepsilon(x_i, rl)^q \right\rangle = \frac{1}{\Lambda - r} \sum_{i=0}^{\Lambda - r} \left[ \varepsilon(x_i, rl) \right]^q , \tag{15}$$

is defined as the $q$th-order singular measure. Obviously, for $q = 0$,

$$M(r, 0) = 1. \tag{16}$$

For $q = 1$,

$$M(r,1) \equiv \left\langle \varepsilon(x_i, rl) \right\rangle = \frac{1}{\Lambda - r} \sum_{i=0}^{\Lambda - r} \left[ \varepsilon(x_i, rl) \right] = \frac{1}{\Lambda - r} \sum_{i=0}^{\Lambda - r} \left[ \frac{1}{r} \sum_{j=i}^{i+r-1} \varepsilon(x_j, l) \right] = 1. \tag{17}$$

The singular measures are computed for all depths. For simplicity, $M(r, q)$ of the three types at 60 m deep is given here (Fig. 13). Near-linear dependence of $\mathrm{Log}_2 [M(r, q)]$ on $\mathrm{Log}_2(r)$ is found for all the three types with different $q$-values from 1 to 6. The straight lines with different slopes show that the singular measures with various $q$ for the upper layer temperature in the WPS satisfies the power law

$$M(r,q) \propto r^{-K(q)}, \quad q \geq 0 , \tag{18}$$

with the power $K(q)$ varying with $q$.

It is noted that for the IS-turbulence type, the power law is broken in the structure function (Fig. 11b) but satisfied in the singular measure (Fig. 13b). This indicates that the internal solitons destroy the self-similarity in stationary features (structural function) and preserve the self-similarity in intermittent features (singular measure). Such a difference may be caused by running average of $r$ normalized absolute gradients for the singular measure. Large perturbations caused by IS propagation are smoothed out and the self-similarity feature preserves.

From Eqs. (16) and (17), we have

$$K(0) = K(1) = 0 . \tag{19}$$

Several characteristics are found from Fig. 13: The power $K(q)$ is a convex function

$$\frac{d^2K(q)}{dq^2} > 0, \tag{20}$$

for all $q$ and

$$K(q) < 0 \quad \text{only if} \quad 0 < q < 1 \tag{21}$$

which reflects the fact that, in this range, taking a $q^{th}$ power necessarily reduces the fluctuation of $\varepsilon(r; x_i)$; and otherwise

$$K(q) \geq 0, \quad \text{if} \quad q \geq 0. \tag{22}$$

Following Chu (2004), we may define a function

$$C(q) = \frac{K(q)}{q-1}. \tag{23}$$

For $q \to 1$, we use *I'Hosptal*'s rule to define a straightforward measure of inhomogeneity in the sense of singular measure

$$C_1 \equiv C(1) = K'(1) \geq 0, \tag{24}$$

which is called the intermittency parameter. The larger the value of $C_1$, the lager the intermittency and singularity the data set has. The $C_1$-value is computed at all depths for the three types. The intermittency parameter $C_1$ varies from 0.25 to 0.6 for the turbulence-dominated type (Fig. 14c), from 0.25 to 0.67 for the IW-turbulence type (Fig. 14a), and 0.29 to 0.84 for the IS-turbulence type (Fig. 14b). The highest intermittency (maximum value of $C_1$) occurs at the up-most part for the turbulence-dominated type, but at the mid-level for the IW-turbulence (60 m deep) and IS-turbulence (65 m deep) types. High $C_1$ values (> 0.7) do not occur for the turbulence-dominated type and IW-turbulence type, but occur in the middle layer (58-73 m, where the thermocline is located, see Fig. 5b) for

the IS-turbulence type. This indicates that the internal solitons generate high intermittency around the thermocline.

## 8. Some Explanation

One may ask: What is the reason causing the multifractal characteristics of the structural function break in the IS-turbulence with coherent structures? Why are the multifractal characteristics broken? Since the major task of this paper is to analyze the high-resolution temperature data, we only present some simple explanation rather than thorough mathematical derivation.

The total energy of the internal waves may be represented as an integral over spectral energy density,

$$E = \int E(\mathbf{k}, m) d\mathbf{k} dm \,, \tag{25}$$

where **k** and m are the horizontal components of wave vector. Under the assumption of horizontal isotropy, Garrett and Munk proposed an empirical expression for the spectral energy density (Garrett and Munk, 1975). Using the Hamitonian formulation, Lvov and Tabak (2001) modified the Garrett-Munk spectrum into

$$E(k,m) = \frac{2fNE}{\pi} \frac{(m/m^*)A(m/m^*)}{N^2k^2 + f^2m^2}, \quad m^* \equiv \gamma(\omega^2 - f^2)^{-\delta/2}, \; A(\lambda) \equiv \frac{t-1}{(1+\lambda)^t}, \tag{26}$$

which represents both internal waves and wave turbulence. Here, $E$ is a constant, quantifying the total energy content of the internal wave spectrum; $f$ is the Coriolis parameter; $\omega$ is the wave frequency; $N$ is the buoyancy frequency; $k = |\mathbf{k}|$, ($t$, $\delta$, $\gamma$) are constants to be determined from observations. Similar multifractal characteristics of the structural function between IW-turbulence and turbulence-dominated types may be due to the energy spectrum (26) representing internal waves and wave turbulence. However,

the internal solitary waves are a class of nonsinusoidal, nonlinear, more-or-less isolated waves of complex shape that maintain their coherence. The internal solitons are usually composed of several oscillations confined to limited region of space, and their energy spectrum is totally different from the internal wave spectrum (26). This might be the reason for the multifractal characteristics of the structural function break at near half of the oscillation period (8 min) in the IS-turbulence with coherent structures. Numerical modeling is needed in the future for fully explain this phenomenon.

## 9. Conclusions

Temperature of the WPS upper layer (to 140 m deep) was sampled with high frequency from July 28 to August 7, 2005 from the coastal monitoring buoy with attached 15 thermistors. The isopycnal displacement is calculated from the temperature field, and the internal waves and solitons were observed.

(1) Three types of thermal variability are identified: IW-turbulence, IS-turbulence, and turbulence-dominated. The power spectra of temperature at all the depths have multi-scale characteristics. The IW-turbulence type has almost the same spectral exponents $\beta$ as the turbulence-dominated type (two scales) with around 0.4 (stationary) for low wavenumbers and nearly 5/3 for high wavenumbers ($\log_2 kL/2 > 4$); but much larger energy $E(k)$ than the turbulence-dominated type. This implies that the energy is distributed in all wavenumbers during the internal wave propagation. The spectrum for the IS-turbulence type is quite different from the two other spectra especially in the spectral exponent $\beta$ (three scales): around 0.4 for low wavenumbers, nearly 4.2 for mid-range wavenumbers, and approximately 5/3 for high wavenumbers.

(2) Without the internal waves and solitons (turbulence-dominated type), the temperature fluctuation has maximum values at the surface, decreases with depth to mid-depths (60-65 m deep), and then increases with depth to 140 m deep. Such depth dependent (decreasing then increasing) pattern preserves during the internal wave propagation during 1000-1500 GMT July 29, 2005. However, this was altered during the internal soliton propagation to a pattern that increases with depth from the surface to 60 m deep, decreases with depth from 60 m deep to 100 m deep, and increases again with depth from 100 m to 140 m deep. The temperature fluctuation enhances with the internal wave and soliton propagation. Between the two, the internal solitons bring larger fluctuations.

(3) The observed temperature profile does not oscillate if there is no internal wave and soliton propagation. It oscillates evidently in the upper layer above 50 m with the internal wave propagation and above 80 m with the internal soliton propagation. The amplitude of the oscillation is much larger during the internal soliton propagation (maximum amplitude around $4^{o}$C) than the internal wave propagation (maximum amplitude around $2^{o}$C).

(4) The structure function satisfies the power law with multifractal characteristics for the IW-turbulence type and turbulence-dominated type, but not for the IS-turbulence type. The internal waves increase the power of the structure function especially for high moments. The internal solitons destroy the multifractal characteristics of the structure function. The power law is broken approximately at the lag of 8 min, which is nearly half period of the IS (with frequency of 4 CPH).

(5) The singular measure (representing the intermittency) satisfies the power law with multifractal characteristics for all the three types (IW-turbulence, IS-turbulence, and turbulence-dominated). The intermittency parameter $C_1$ does not change too much during the internal wave propagation, but increases drastically during the internal soliton propagation. This implies that the internal waves do not generate extra intermittency, but the internal solitons generate high intermittency.

(6) The multifractal analysis provides a useful framework to analyze ocean data when complex nonlinear processes exist. For the data collected from the CMB with attached thermistors, it clearly shows different effects on the upper ocean multifractal thermal structure between internal wave and internal soliton propagation. The physical mechanisms causing these different effects need to be further explored. Besides, the universality of the multifractal properties obtained in this paper should be tested in different oceans and fluid phenomena especially the breakdown of multifractal characteristics in the IS-turbulence type when coherent structures appear in turbulent fields.

**Acknowledgments.** This work was funded by the Office of Naval Research, Naval Oceanographic Office, and the Naval Postgraduate School.

## References

Chu, P.C., 2004: Multifractal thermal characteristics of the southwestern GIN Sea upper layer. Chaos, Solitons and Fractals, 19 (2), 275-284.

Chu, P.C., and R.F. Li, 2000: South China Sea isopycnal surface circulation. Journal of Physical Oceanography, 30, 2419-2438.

Chu, P.C., and C.W. Fan, 2001: Low salinity, cool-core cyclonic eddy detected northwest of Luzonduring the South China Sea Monsoon Experiment (SCSMEX) in July 1998. Journal of Ocenography, 57, 549-563.

Chu, P.C., L. Ivanov, L. Kantha, O. Melnichenko, and Y. Poberezhny, 2002: Power law decay in model predictability skill. Geophysical Research Letters, 29 (15), 10.1029/2002GLO14891.

Chu, P.C., and C.-P. Hsieh, 2007: Multifractal thermal characteristics of the western Philippine Sea upper layer. Indian J. Mar. Sci., in press.

Desaubles Y., and M. C. Gregg, 1981: Reversible and irreversible finestructure. J. Phys. Oceanogr., 11, 541-556.

Garrett, C. J. R., and W. H. Munk, 1975: Space-time scales of internal waves, a progress report. J. Geophys. Res. **80**, 281-297.

Liu, A. K., Y. S. Chang, M.-K. Hsu, and N. K. Liang, 1998: Evolution of nonlinear internal waves in the East and South China Seas. J. Geophys. Res., 103, 7995–8008.

Lvov, Y.V., and E.G. Tabak, 2001: Hamiltonian formalism and the Garrett-Munk spectrum of internal waves in the ocean. Phys. Rev. Lett., 87, 168501-1 to 168501-4, DOI: 10.1103/PhysRevLett.87.168501.

Nitani, H., 1972: Beginning of Kuroshio. In Kuroshio: Its Physical Aspects, edited by H. Stommel and K. Yoshida, University of Tokyo Press, Tokyo, 129-163.

Ramp, S. R., T.-Y. Tang, T. F. Duda, J. F. Lynch, A. K. Liu, C.-S. Chiu, F. L. Bahr, H.-R. Kim, and Y.-J. Yang, 2004: Internal Solitons in the Northeastern South China Sea Part I: Sources and Deep Water Propagation, IEEE J. Oceanic Eng., 29, 1157-1180.

Su, J.L., and V.B. Lobanov, 1998: Eastern Asia, Kamchatka to the eastern coast of the Philippines coastal section (10, w). In The Sea, Vol 11, the Global Coastal Ocean, edited by A. R. Robinson and K. H. Brink, John Wiley and Sons, Inc., New York, 415-427.

Xu, J.P., and J.L. Su, 1997: Hydrographic analysis on the intrusion of the Kuroshio into the South China Sea, Part 2, Observational results during the cruise from August to September in 1994. Tropic Oceanol., 16 (2), 1-23 (in Chinese).

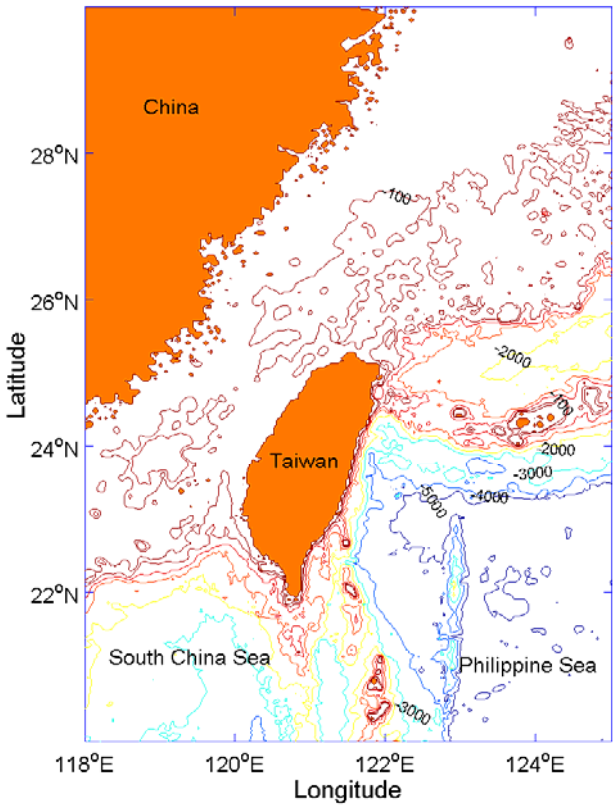


Figure1. Topography of the western Philippine Sea and surrounding areas.

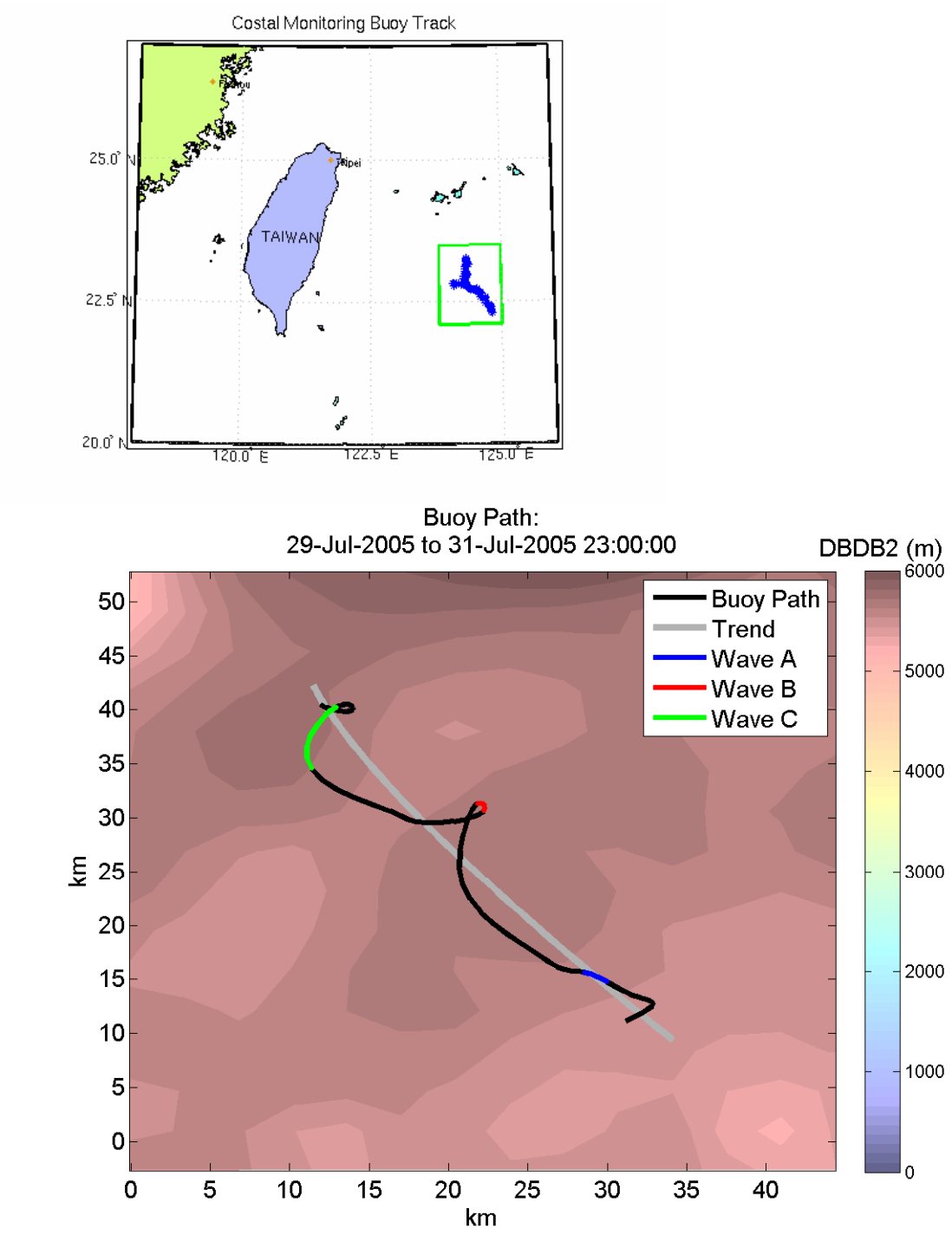


Figure 2. Track of CMB (from July 28 to August 7, 2005) deployed by the Naval Oceanographic Office.

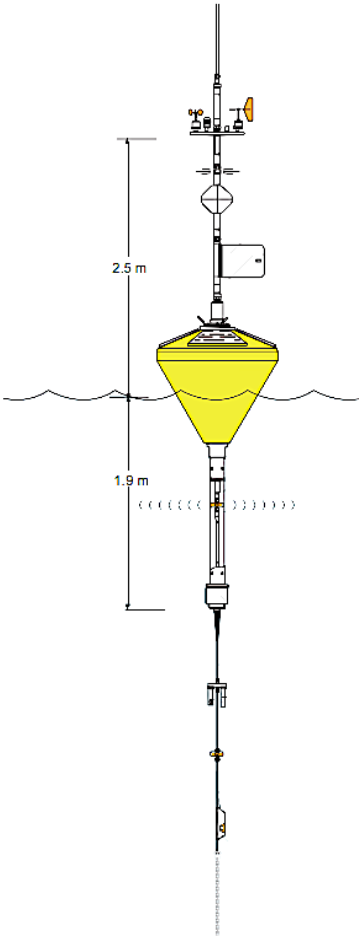


Figure 3. The Coastal Monitoring Buoy used in the WPS survey. Fifteen thermistors are attached to a wire rope extending from the code of CMB (20 m deep) to 140 m with high frequency sampling rate (every 15 sec).

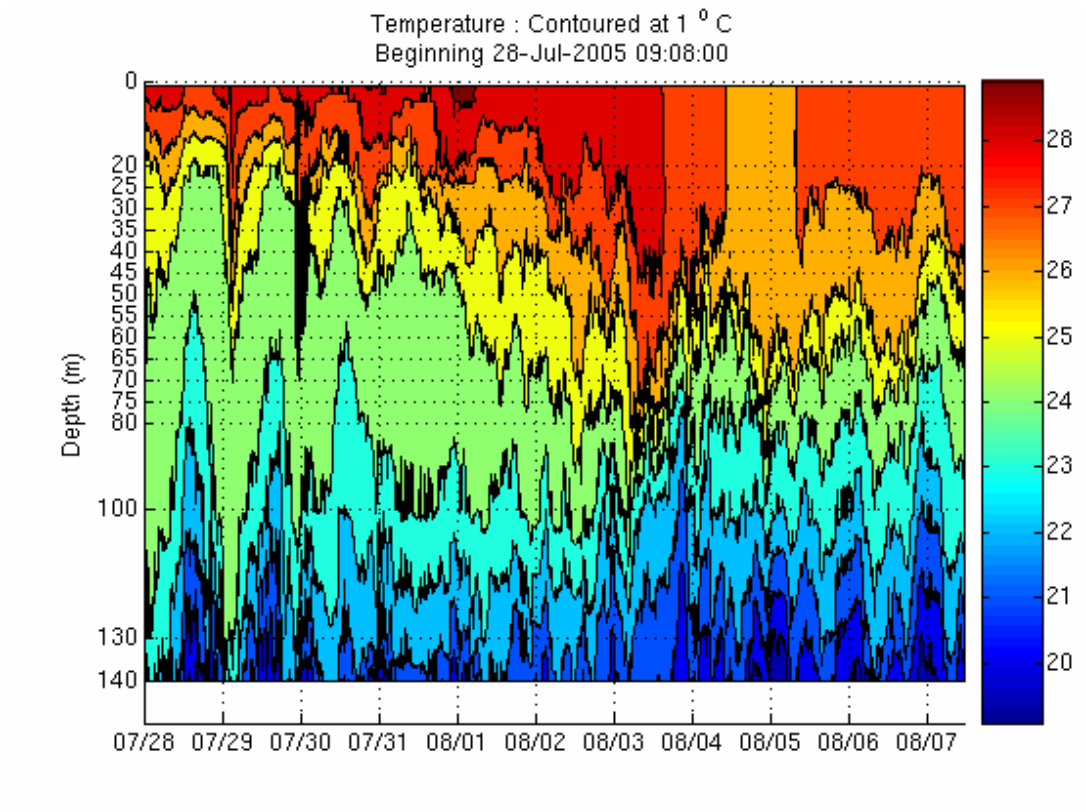


Figure 4. Time-depth cross section of temperature obtained from the CMB data collected along the track shown in Figure 2.

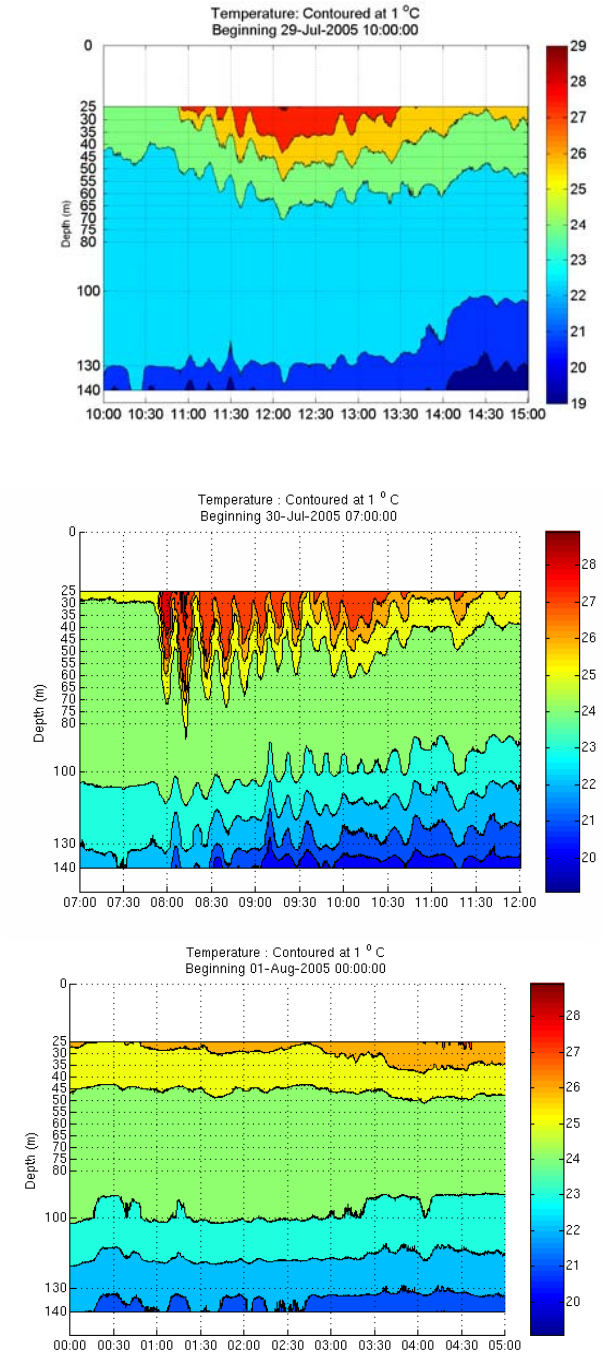


Figure 5. Time-depth cross section of temperature on (a) 1000-1500 GMT July 29 (IW-turbulence), (b) 0700-1200 GMT July 30 (IS-turbulence), and (c) 0000- 0500 GMT August 1 (turbulence-dominated) obtained from the CMB data collected along the track shown in Figure 2.

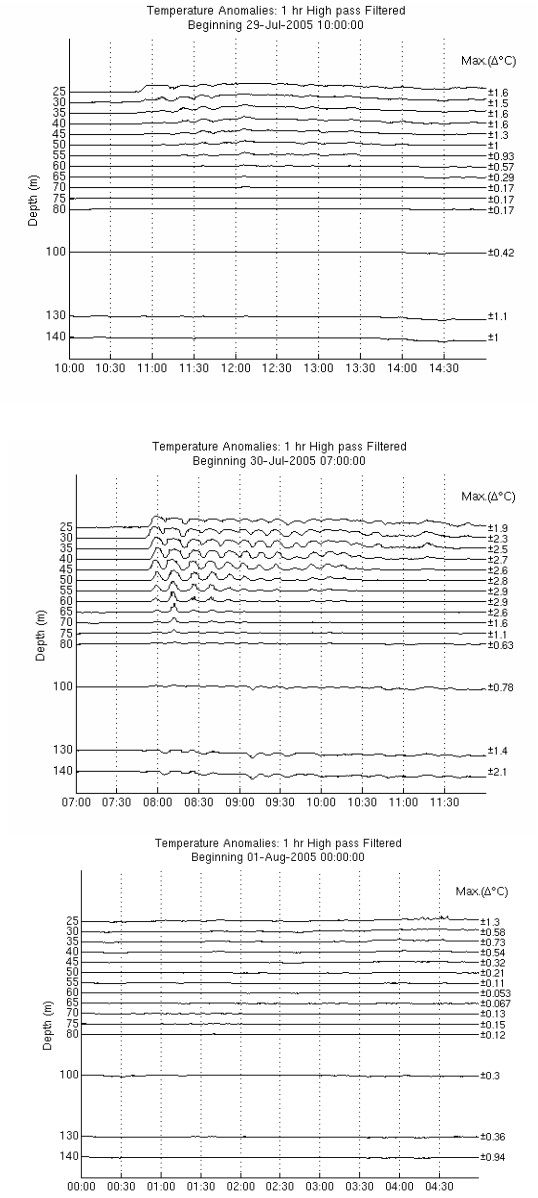


Figure 6. Temporal variation of temperature anomaly at the thermistor depth on (a) 1000-1500 GMT July 29 (IW-turbulence), (b) 0700-1200 GMT July 30 (IS-turbulence), and (c) 0000- 0500 GMT August 1 (turbulence-dominated), 2005.

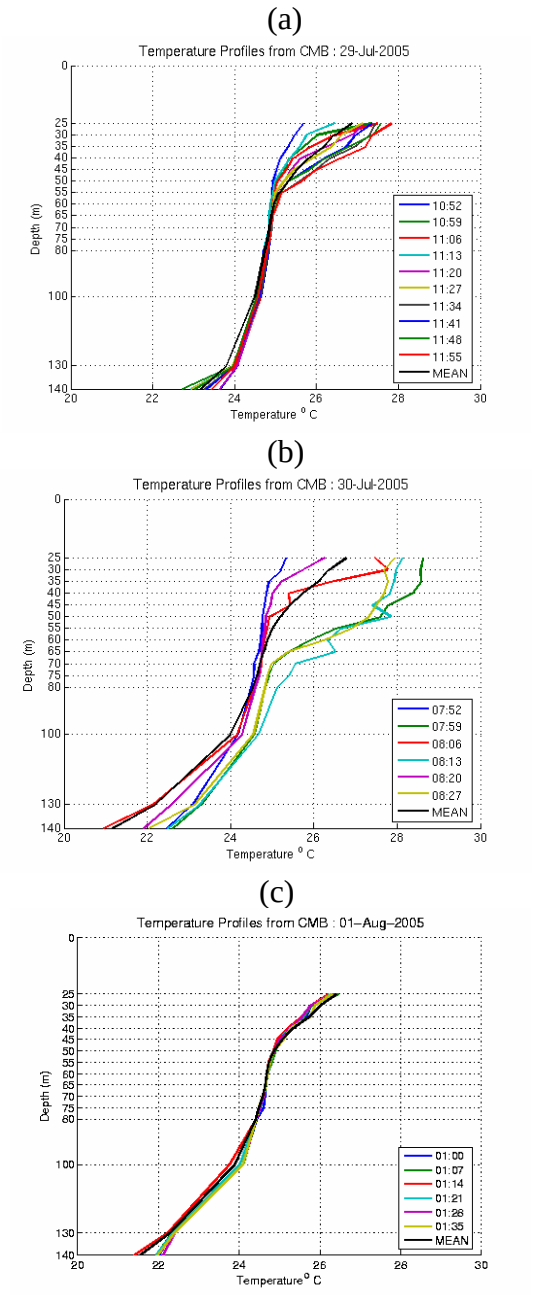


Figure 7. Temporally varying temperature profiles observed from CMB thermistors on (a) 1000-1500 GMT July 29 (IW-turbulence), (b) 0700-1200 GMT July 30 (IS-turbulence), and (c) 0000- 0500 GMT August 1 (turbulence-dominated), 2005. The oscillation of the temperature profiles is found in (a) and (b) with period around 14 min, but not found in (c). The amplitude of the oscillation is much larger in (b) than in (a).

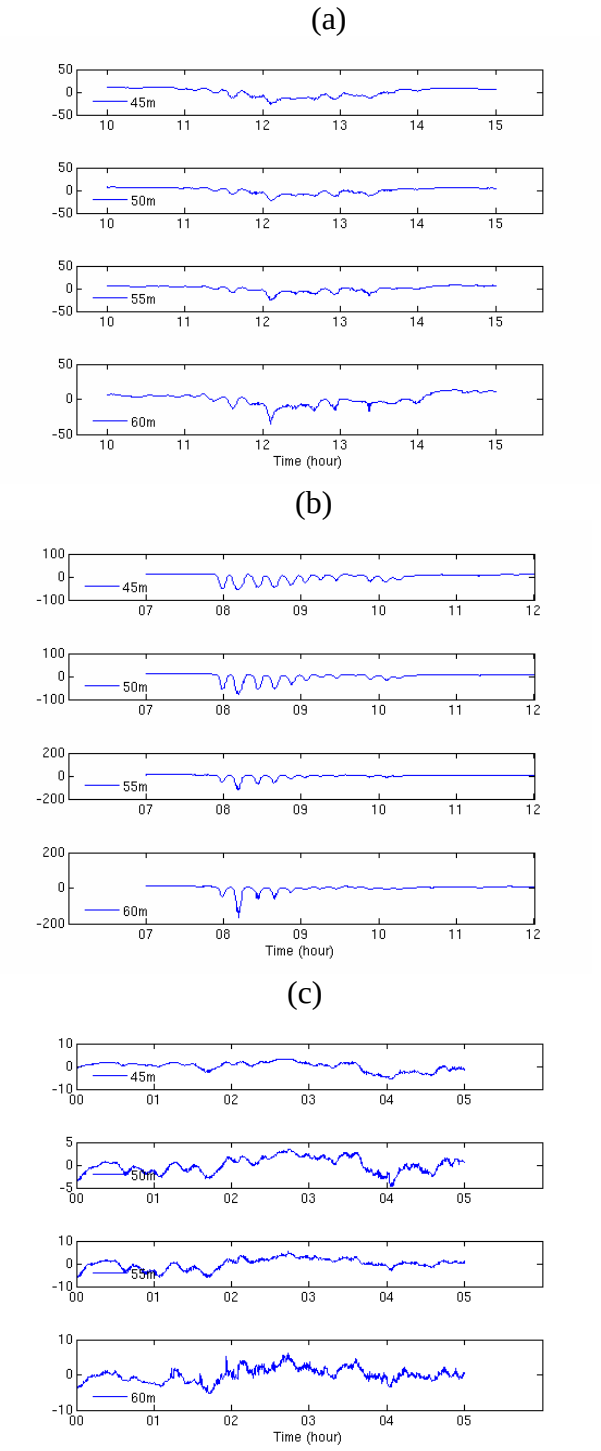


Figure 8. Isopycnal displacements measured by thermistors at 45 m, 50 m, 55 m, and 60 m depths on (a) 1000-1500 GMT July 29 (IW-turbulence), (b) 0700-1200 GMT July 30 (IS-turbulence), and (c) 0000- 0500 GMT August 1 (turbulence-dominated), 2005. The isopycnal displacement is the strongest in (b) with a maximum value of around 160 m at 80 m depth, and in (b) and the weakest in (c) with maximum value less than 5 m.

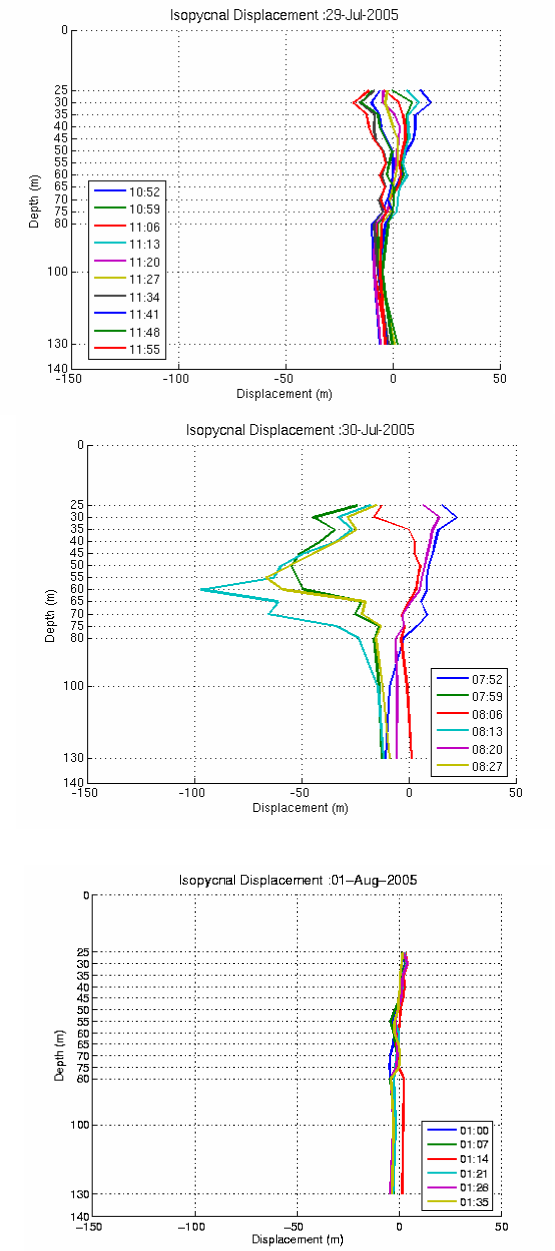


Figure 9. Temporally varying isopycnal displacement identified from CMB thermistors on (a) 1000-1500 GMT July 29 (IW-turbulence), (b) 0700-1200 GMT July 30 (IS-turbulence), and (c) 0000- 0500 GMT August 1 (turbulence-dominated), 2005. The oscillation of the isopycnal displacement is found in (a) and (b) with period around 14 min, but not in (c). The amplitude of the oscillation is much larger in (b) than in (a).

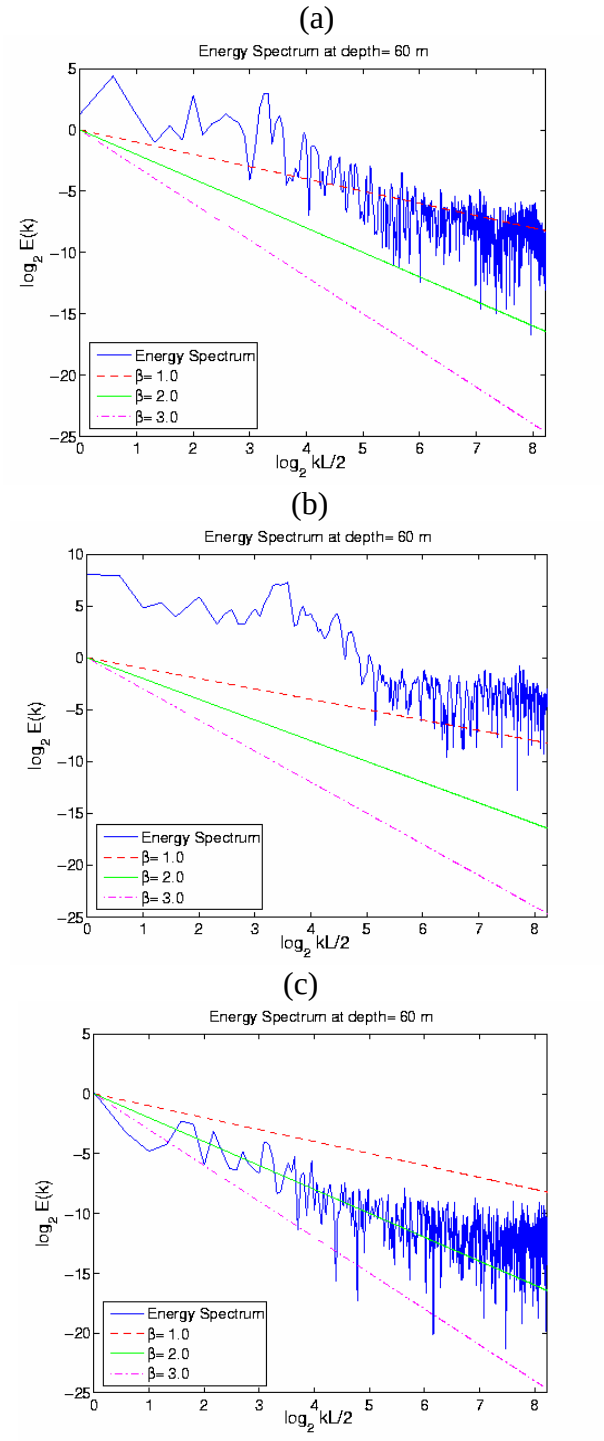


Figure 10. Power spectra of temperature at 60 m deep on (a) 1000-1500 GMT July 29 (IW-turbulence), (b) 0700-1200 GMT July 30 (IS-turbulence), and (c) 0000- 0500 GMT August 1 (turbulence-dominated), 2005.

(a)

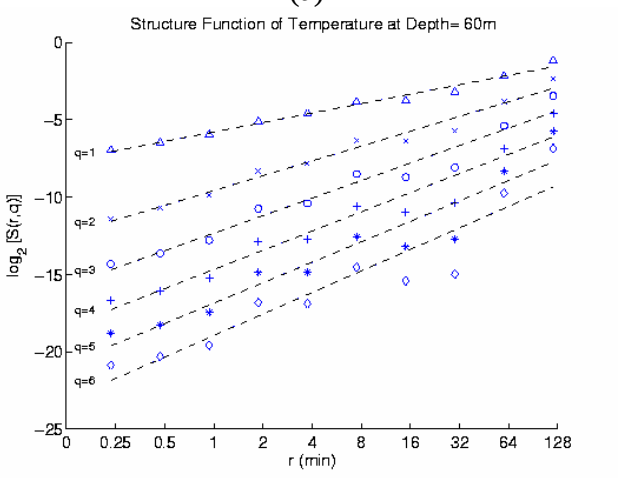


(b)

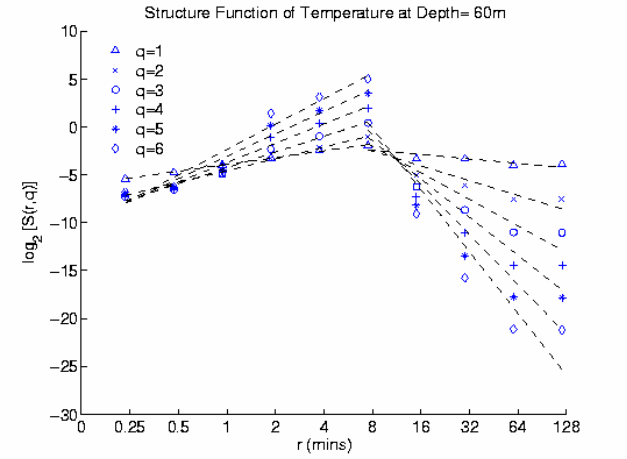


(c)

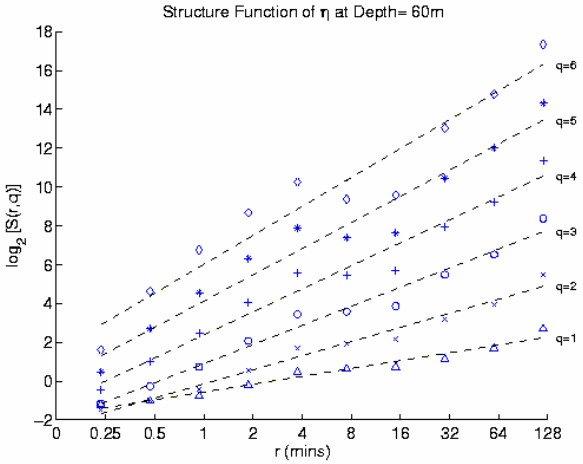


Figure 11. Statistical structure functions of temperature at 60 m deep on (a) 1000-1500 GMT July 29 (IW-turbulence), (b) 0700-1200 GMT July 30 (IS-turbulence), and (c) 0000- 0500 GMT August 1 (turbulence-dominated), 2005.

(a)

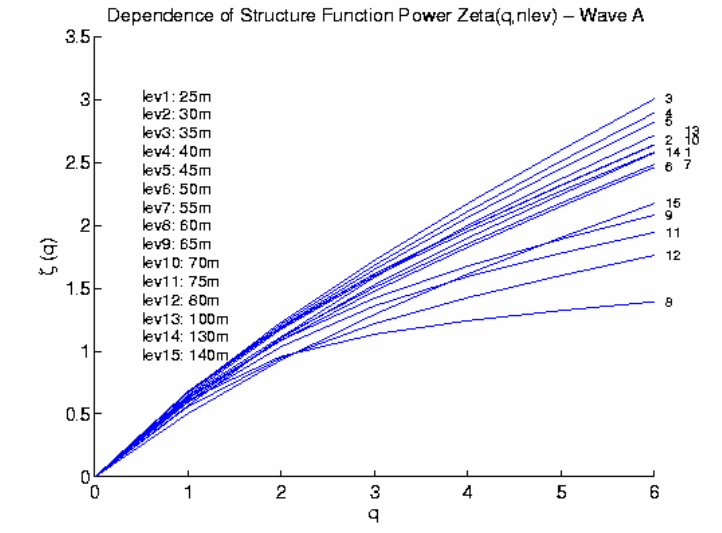


(b)

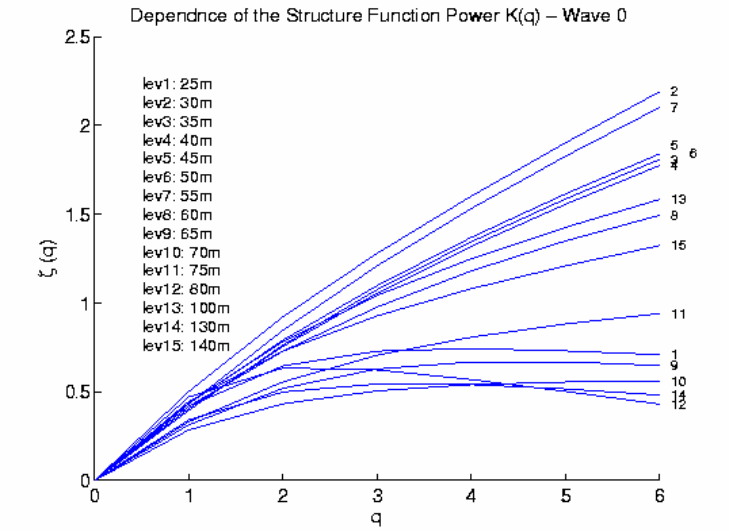


Figure 12. Dependence of the structure function's power, $\zeta(q)$, on $q$ and depth for (a) 1000-1500 GMT July 29 (IW-turbulence), and (b) 0000- 0500 GMT August 1 (turbulence-dominated), 2005.

(a)

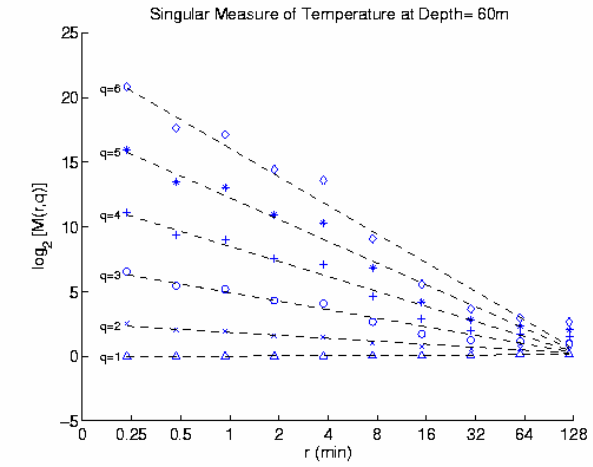


(b)

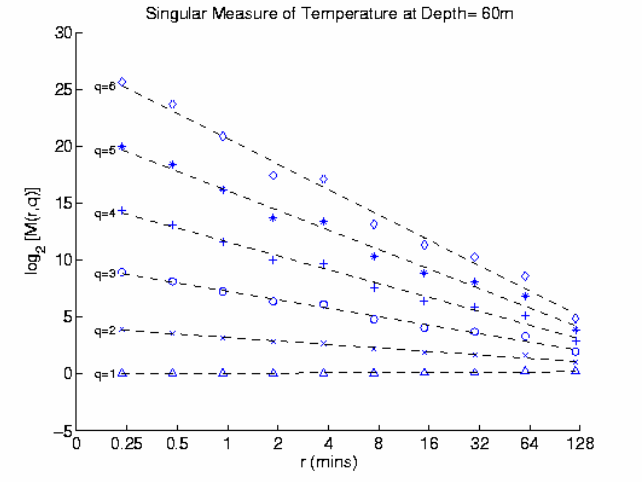


(c)

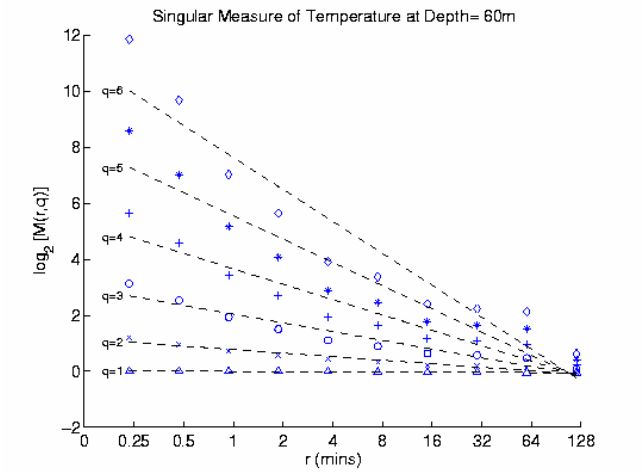


Figure 13. Singular measures of temperature at 60 m deep on (a) 1000-1500 GMT July 29 (IW-turbulence), (b) 0700-1200 GMT July 30 (IS-turbulence), and (c) 0000- 0500 GMT August 1 (turbulence-dominated), 2005.

(a)

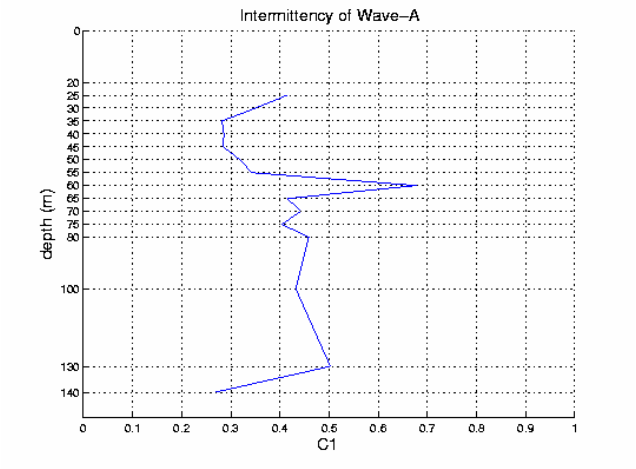


(b)

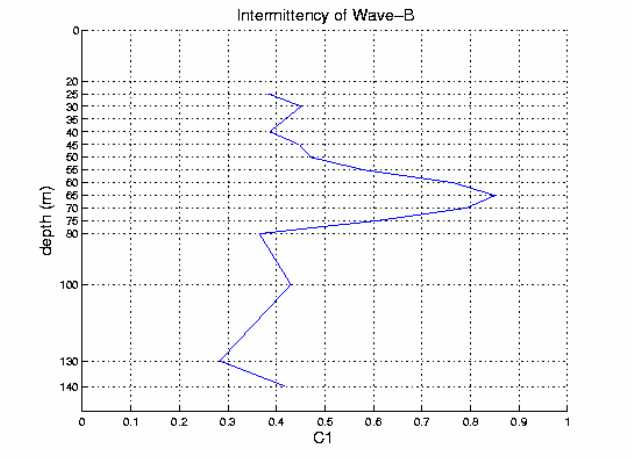


(c)

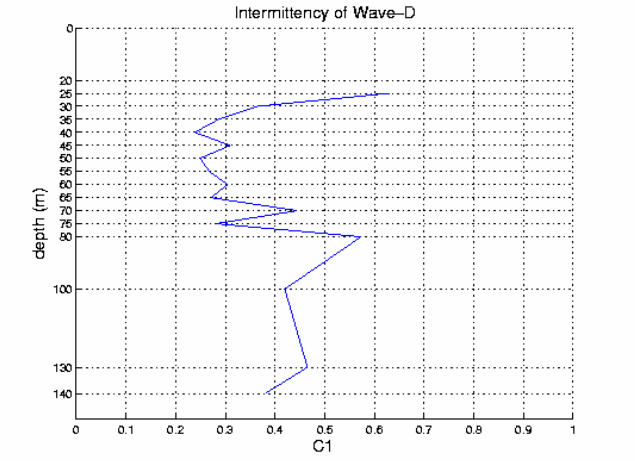


Figure 14. Depth dependent intermittency parameter $C_1$ on (a) 1000-1500 GMT July 29 (IW-turbulence), (b) 0700-1200 GMT July 30 (IS-turbulence), and (c) 0000- 0500 GMT August 1 (turbulence-dominated), 2005.